JOURNAL OF PROPULSION AND POWER
Vol. 20, No. 4, July–August 2004

Performance Theory of Diagonal Conducting Wall Magnetohydrodynamic Accelerators

Ron J. Litchford*
NASA Marshall Space Flight Center, Huntsville, Alabama 35812

The theoretical performance of diagonal conducting wall crossed field accelerators is examined on the basis of an infinite segmentation assumption using a cross-plane averaged generalized Ohm's law for a partially ionized gas, including ion slip. The desired accelerator performance relationships are derived from the cross-plane averaged Ohm's law by the imposition of appropriate configuration and power-connection constraints. A current dependent effective voltage drop model is also incorporated to account for cold-wall boundary-layer effects, including gasdynamic variations, discharge constriction, and electrode falls. Definition of dimensionless electric fields and current densities lead to the construction of graphical performance diagrams, which further illuminate the rudimentary behavior of crossed field accelerator operation.

Nomenclature

A	=	cross-sectional area, hw
A_f	=	slanted area, $A\tan\theta$
a	=	conductivity power law exponent
$\boldsymbol{B}$	=	magnetic field strength, induction
b	=	ion slip factor
$\boldsymbol{E}$	=	electric field, ($\mathcal{E}$, dimensionless)
h	=	channel height
I	=	total current, ($\mathcal{I}$, dimensionless)
$\boldsymbol{j}$	=	current density, ($\mathcal{J}$, dimensionless)
L	=	channel length
M	=	Mach number
m	=	thermal boundary-layer power law exponent
n	=	velocity boundary-layer power law exponent
P	=	power density, ($\mathcal{P}$, dimensionless)
R	=	load resistance
T	=	temperature
$\boldsymbol{u}$	=	velocity
V	=	voltage
w	=	channel width
α	=	Hall angle, $\tan^{-1}\Omega$
β	=	Hall parameter
Δ	=	dimensionless voltage drop, E_d/uB
δ	=	boundary-layer thickness
η	=	electrical efficiency
θ	=	electric field angle, $\tan^{-1}\varphi$
θ_w	=	diagonalization or wall angle, $\pi/2-\theta$
ξ	=	dimensionless height parameter, y/δ
Σ	=	effective electrical conductivity
σ	=	scalar electrical conductivity
φ	=	electric field direction, $\tan\theta$
Ω	=	effective Hall parameter
ω	=	conductivity ratio

Introduction

HISTORICALLY, interest in magnetohydrodynamic (MHD) devices has centered on their use as electrical generators in commercial central power plants and mobile burst power systems. The primary attraction for central power is associated with the attainment of higher peak cycle temperatures, which point to significant improvements in overall plant efficiency. The attraction for mobile pulse power, particularly airborne military needs, derives from their intrinsic high power density characteristics. It should be recognized that equally important, though less noted, attractions exist for accelerator configurations as well.

Two major identifiable uses for crossed-field MHD accelerators are as propulsive devices and hypersonic aerodynamic test facilities. Litchford et al. discuss the operational attributes that are of particular significance to these applications and provide an in-depth historical perspective of their technological development.[1]

From a fundamental point of view, the essential argument favoring utilization of a Lorentz force acceleration mechanism is the ability to avoid inherent physical limitations encountered with pure thermal approaches, namely, material thermal limits and ionization/dissociation losses. Simply put, it is more effective to transfer electrical energy into directed kinetic energy instead of first degrading it into thermal energy. Crossed-field acceleration is of special interest in these cases because of its unique capacity for processing large amounts of power under conditions of high mass throughput.

Past emphasis on generator configurations has led to a substantial theoretical and experimental basis for understanding their performance and operational nuances. However, a similar level of understanding has yet to be acquired for accelerator configurations, despite a strong growing interest in their potential aerospace applications.

The standard theoretical approach for describing the interaction of an electrically conducting gas with applied electric and magnetic fields relies on application of a Cowling–Schlueter type generalized Ohm's law for a partially ionized, electrically neutral gas. Powers et al., for instance, used a cross plane averaged form of the generalized Ohm's law and developed a graphical-based methodology for describing the general performance characteristics of both MHD accelerators and generators.[2]

This classical model has proven to be extremely useful in illuminating the basic operational behavior of MHD devices; but its practical utility is hampered by a critical limitation. That is, the theory assumes a constant near-electrode voltage drop, whereas experience has shown that the magnitude of the near-electrode voltage drop exhibits a significant load current dependency.

Various theoretical refinements of this nature have been forthcoming, but solely within the context of generator configurations. Wu, for example, introduced an effective voltage drop parameter, accounted for its load current dependency, and examined the resulting impact on diagonal conducting wall (DCW) generator performance.[3] The MHD research group at the Max Plank Institut fuer Plasmaphysik took a similar approach to the problem using a cross-plane-averaged Ohm's law, as specialized for a DCW generator configuration.[4]

Presented as Paper 2003-4284 at the AIAA 34th Plasmadynamics and Lasers Conference, Orlando, FL, 23 June 2003; received 9 July 2003; revision received 17 November 2003; accepted for publication 19 November 2003.

*Head, Energetics Research Group, Propulsion Research Laboratory/TD40. Associate Fellow AIAA.

It is widely recognized, of course, that the current and electric field structure in MHD devices is inherently three-dimensional and that spatial separation of physical processes is not warranted, in general. As a matter of recourse, one could mount a brute force attack on the problem and perform a complete three-dimensional numerical analysis of the flow and electrical structure in the duct, assuming adequate computing resources are available. Alternatively, one could invoke an infinite segmentation assumption, which assumes the streamwise variation in electrical properties is small in comparison to transverse variations, and couple an approximate cross-plane electrical model with a three-dimensional flow analysis, as exemplified for generator configurations by Bityurin et al.[5] and Ahluwalia et al.[6] Each approach has its merits and drawbacks, and experience has shown that each level of approximation is useful in fulfilling certain design and analysis needs.

The purpose of this paper is to reexamine the classical theory and extend it for cross-field accelerator configurations with inclusion of a current dependent near-electrode voltage drop model. This particular refinement of the classical theory, although generally recognized as a straightforward theoretical extension, has not appeared explicitly in the literature, and it is believed that the resulting development can yield practical insight into the basic operational characteristics of these important devices. Moreover, it is hoped that this work may serve as a convenient and compact resource for future design practitioners.

Crossed-Field Accelerator Configurations

Various linear crossed-field MHD accelerator configurations are conceivable (Fig. 1), although the optimal configuration depends on the ultimate application need. The Hall configuration, for example, is generally more effective for low-density flows, under very high Hall parameter conditions, whereas the segmented Faraday configuration yields superior performance for high-density flows. A significant disadvantage of the Faraday configuration, however, is the separate power conditioning required for each electrode pair leading to a heavy, complex, and expensive system.

Alternative two-terminal loading schemes have been proposed to avoid the complications of multi-terminal connections, while attempting to compensate for the effects associated with a finite Hall parameter. De Montardy, for instance, suggested the series connected scheme in which a segmented Faraday channel is externally diagonalized.[7] Dicks later extended this approach to a DCW configuration in which slanted window-frame-like electrode elements are stacked with thin insulators to form a complete channel.[8,9] The DCW configuration is a conceptually simple design and incurs no performance penalties in comparison to the series connected device.

Hence, theoretical development is focused on the DCW accelerator configuration because it has the greatest practical relevance. The performance characteristics of the alternative crossed-field configurations can be subsequently deduced as special or extreme cases of the DCW configuration.

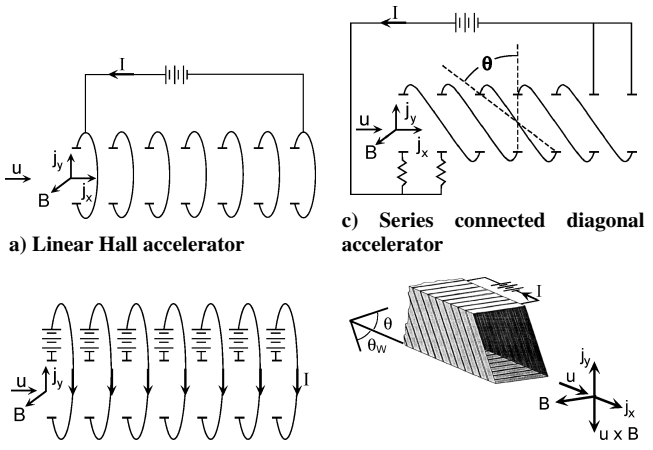

a) Linear Hall accelerator

c) Series connected diagonal accelerator

b) Segmented Faraday accelerator

d) Diagonal conducting wall accelerator

Fig. 1 Composite graphic of alternative cross-field MHD accelerator configurations.

Generalized Ohm's Law

The local current density $\boldsymbol{j}$ in a partially ionized, electrically neutral gas may be determined from a Cowling-Schlueter type generalized Ohm's law (see Refs. 10–14). For application to typical MHD devices, it is useful to adopt the simplified form derived by Rosa, which includes ion slip but neglects electron pressure gradients[15]:

$$\boldsymbol{j} = \sigma \boldsymbol{E}' - (\beta_e/B)\boldsymbol{j} \times \boldsymbol{B} + \left(\beta_e \beta_i \big/ B^2\right)(\boldsymbol{j} \times \boldsymbol{B}) \times \boldsymbol{B} \tag{1}$$

Here, $\mathbf{E}'$ is the generalized electric field intensity relative to axes moving with gas velocity $\boldsymbol{u}$ and β_e and β_i are the electron and ion Hall parameters, respectively. The Hall effect and ion slip are introduced by the second and third terms on the right-hand side.

As a practical matter, we define the generalized electric field $\boldsymbol{E}'$ in terms of the electric field in the laboratory frame $\boldsymbol{E}$, the motional emf $\boldsymbol{u} \times \boldsymbol{B}$, and an equivalent electric field $\boldsymbol{E}_d$ that accounts for the near-electrode voltage drop V_d, that is, $E_d = V_d/h$, inside the boundary layer:

$$\boldsymbol{E}' = \boldsymbol{E} + \boldsymbol{u} \times \boldsymbol{B} - \boldsymbol{E}_d \tag{2}$$

Note that the equivalent electric field is applied only in a direction transverse to the magnetic field vector and the streamwise velocity vector. It is always directed in opposition to the transverse current j_y.

For the special case in which no current flows along the magnetic field lines ($j_z = 0$), it is readily shown that Eq. (1) reduces to the compact form

$$\boldsymbol{j} = \Sigma \boldsymbol{E}' - (\Omega/B)\boldsymbol{j} \times \boldsymbol{B} \tag{3}$$

where we have introduced two new parameters

$$\Sigma = \sigma/(1 + \beta_e \beta_i) = \sigma/(1 + b) \tag{4}$$

$$\Omega = \beta_e/(1 + \beta_e \beta_i) = \beta_e/(1 + b) \tag{5}$$

In many cases, the ion slip factor $b = \beta_e \beta_i$ is negligible, and further simplification can be obtained as $\Sigma \to \sigma$ and $\Omega \to \beta_e$.

Mean Ohm's Law

Many of the interesting phenomena that occur in high-interaction MHD devices such as velocity overshoots in the sidewall boundary layer, flow asymmetries, and generation of intense secondary flows in the cross plane are three dimensional in nature. Therefore, high-fidelity performance predictions ultimately require three-dimensional numerical analyses of the combined flow and electrical structure. On the other hand, simplified approaches based on spatial decoupling or reduced spatial dimensions can also yield useful results if all critical physical effects are accounted for in an appropriate fashion.

Exact theoretical treatment requires consideration of the fundamental equations of MHD and Maxwell's electromagnetic equations, thereby leading to a system of coupled differential equations. Here, we invoke the infinite segmentation assumption and assume that all parameters in the generalized Ohm's law can be effectively represented by their cross-plane-averaged values and are dependent on the x coordinate only.

The dimensionless voltage drop parameter $\Delta = E_d/uB = Vd/uBh$, which incorporates all voltage losses associated with the electrode boundary layer, may be introduced into the generalized Ohm's law to obtain the following component relations:

$$j_x = \Sigma E_x - \Omega j_y \tag{6}$$

$$j_y = \Sigma E_y - \Sigma uB\,(1 + \Delta) + \Omega j_x \tag{7}$$

Table 1 Summary of electrical parameter relationships for diagonalized cross-field MHD devices[a]

Electrical parameter	In terms of applied electric field E_x	In terms of applied electric current I
j_x	$\dfrac{(1-\Omega\varphi)\Sigma E_x + \Omega\Sigma uB(1+\Delta)}{1+\Omega^2}$	$\dfrac{(1-\Omega\varphi)I/A + \varphi\Sigma uB(1+\Delta)}{1+\varphi^2}$
j_y	$\dfrac{(\Omega+\varphi)\Sigma E_x - \Sigma uB(1+\Delta)}{1+\Omega^2}$	$\dfrac{(\Omega+\varphi)I/A - \Sigma uB(1+\Delta)}{1+\varphi^2}$
E_x	E_x	$\dfrac{(1+\Omega^2)I/A + (\varphi-\Omega)\Sigma uB(1+\Delta)}{\Sigma(1+\varphi^2)}$
E_y	φE_x	φE_x
I	$\dfrac{(1+\varphi^2)\Sigma E_x A + (\Omega-\varphi)\Sigma uB(1+\Delta)A}{1+\Omega^2}$	I

[a]The sign of φ and Δ depends on the mode of operation: generator mode, $\varphi < 0$ and $-1 \le \Delta \le 0$ and accelerator mode, $\varphi > 0$ and $\Delta \ge 0$.

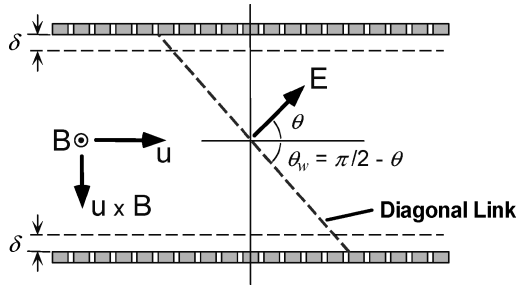

Fig. 2 Orientation of field vectors in a diagonally connected cross-field accelerator.

Equations (6) and (7) may also be combined to obtain the inverse expressions for j_x and j_y in terms of the local electric field components:

$$j_x = [\Sigma/(1+\Omega^2)][E_x - \Omega E_y] + [\Omega/(1+\Omega^2)]\Sigma uB(1+\Delta) \quad (8)$$

$$j_y = [\Sigma/(1+\Omega^2)][\Omega E_x + E_y] - [1/(1+\Omega^2)]\Sigma uB(1+\Delta) \quad (9)$$

Performance Model

Diagonal Constraint

Completion of the electrical model requires consideration of external loading conditions. In the case of a diagonally linked device (Fig. 2), the electric field is forced to align perpendicular to the diagonal short such that

$$E_y/E_x = \tan\theta = \varphi \quad (10)$$

It follows that the diagonalization or wall angle is given by $\theta_w = \pi/2 - \theta$. The sign of φ depends on the mode of operation. For an accelerator, $\boldsymbol{u} \times \boldsymbol{B}$ opposes j_y, $0 < \theta < \pi/2$, and $\varphi > 0$. For a generator, $\boldsymbol{u} \times \boldsymbol{B}$ aligns with j_y, $-\pi/2 < \theta < 0$ and $\varphi < 0$.

The total two-terminal current I for an MHD device with diagonally linked electrode pairs is given by

$$I = \int_{A_f} \boldsymbol{j} \cdot \mathrm{d}\boldsymbol{A}_f = \boldsymbol{j} \cdot \boldsymbol{n} A_f \quad (11)$$

where the integration is over the entire slanted area A_f. In component form,

$$I = (j_x + \tan\theta j_y)A = (j_x + \varphi j_y)A \quad (12)$$

Electrical Parameter Relationships

A complete set of equations now exists for determination of the cross-plane electrical characteristics. In general, either I or E_x may be specified, which allows the remaining unknown electrical parameters to be deduced from Eqs. (6), (7), (10), and (12) in conjunction with appropriate material functions.

The resulting performance relationships for DCW accelerators are listed in Table 1 using both E_x and I as the independent variable.

The governing relations for generator performance are recovered when both φ and Δ are less than zero and $I = -E_x L/R$, where R is the load resistance and L is the channel length over which the load is applied. Note also that the governing relations for a linear Hall channel configuration are recovered in the extreme case $\varphi = 0$.

Mean Power Parameters

Ultimately, we seek to deduce suitably averaged power parameters from the resulting cross-plane electrical model. The quantities $\boldsymbol{j} \cdot \boldsymbol{E}$ and $(\boldsymbol{j} \times \boldsymbol{B})_x$, for instance, may be used to determine the power density, push power, dissipated power, and electrical efficiency of a device.

Power Density

The electrical power density at any cross section of the duct is defined by

$$P = \boldsymbol{j} \cdot \boldsymbol{E} = (I/A_f)\sqrt{E_x^2 + E_y^2} \quad (13)$$

The elimination of E_y by the use of Eq. (10) yields

$$P = (I/A_f)\sqrt{E_x^2 + \varphi^2 E_x^2} = (I E_x/A_f)\sqrt{1+\varphi^2} \quad (14)$$

However, $A_f = A\sqrt{(1+\varphi^2)}$, and we obtain the working form

$$P = I E_x/A \quad (15)$$

Push Power

The streamwise Lorentz body force component at any cross section is defined as

$$(\boldsymbol{j} \times \boldsymbol{B})_x = j_y B \quad (16)$$

and the push power associated with this Lorentz body force is given by

$$P_p = \boldsymbol{u} \cdot (\boldsymbol{j} \times \boldsymbol{B})_x = u j_y B \quad (17)$$

Dissipated Power

The power density of an MHD device must exceed the Lorentz force push power because the internal resistance to current flow leads to ohmic heating. This can be demonstrated by the use of the dot product of $\boldsymbol{j}$ with the generalized Ohm's law, as defined by Eq. (3),

$$\boldsymbol{j} \cdot \boldsymbol{j} = \Sigma[\boldsymbol{j} \cdot \boldsymbol{E} + \boldsymbol{j} \cdot (\boldsymbol{u} \times \boldsymbol{B}) - \boldsymbol{j} \cdot \boldsymbol{E}_d] - (\Omega/B)\boldsymbol{j} \cdot (\boldsymbol{j} \times \boldsymbol{B}) \quad (18)$$

Because $j_z = 0$, the last term is identically zero and we obtain

$$(\boldsymbol{j} \cdot \boldsymbol{j})/\Sigma = \boldsymbol{j} \cdot \boldsymbol{E} - \boldsymbol{u} \cdot \boldsymbol{j} \times \boldsymbol{B} - \boldsymbol{j} \cdot \boldsymbol{E}_d = P - P_p - j_y u B \Delta \quad (19)$$

Table 2 Summary of mean power relationships for diagonalized cross-field MHD devices[a]

Power parameter	In terms of applied electric field E_x	In terms of applied electric current I
$P = \boldsymbol{j}\cdot\boldsymbol{E}$	$\Sigma E_x^2\left[\dfrac{(1+\varphi^2)+(\Omega-\varphi)uB(1+\Delta)/E_x}{1+\Omega^2}\right]$	$\dfrac{I^2}{\Sigma A^2}\left[\dfrac{(1+\Omega^2)+(\varphi-\Omega)\Sigma uB(1+\Delta)A/I}{1+\varphi^2}\right]$
$P_p = \boldsymbol{u}\cdot(\boldsymbol{j}\times\boldsymbol{B})_x$	$\Sigma E_x uB\left[\dfrac{(\Omega+\varphi)-uB(1+\Delta)/E_x}{1+\Omega^2}\right]$	$\dfrac{uBI}{A}\left[\dfrac{(\Omega+\varphi)-\Sigma uB(1+\Delta)A/I}{1+\varphi^2}\right]$
$\eta_a = \dfrac{\boldsymbol{u}\cdot(\boldsymbol{j}\times\boldsymbol{B})_x}{\boldsymbol{j}\cdot\boldsymbol{E}} = \dfrac{1}{\eta_g}$	$\dfrac{uB}{E_x}\left[\dfrac{(\Omega+\varphi)-uB(1+\Delta)/E_x}{(1+\varphi^2)+(\Omega-\varphi)uB(1+\Delta)/E_x}\right]$	$\dfrac{\Sigma uB}{I/A}\left[\dfrac{(\Omega+\varphi)-\Sigma uB(1+\Delta)A/I}{(1+\Omega^2)+(\varphi-\Omega)\Sigma uB(1+\Delta)A/I}\right]$

[a]The sign of φ and Δ depends on the mode of operation: generator mode, $\varphi<0$ and $-1\le\Delta\le 0$ and accelerator mode, $\varphi>0$ and $\Delta\ge 0$.

where $\boldsymbol{j}\cdot\boldsymbol{j}/\Sigma$ is the power dissipated in the core flow region and $\boldsymbol{j}\cdot\boldsymbol{E}_d = j_y E_d = j_y uB\Delta$ represents the power dissipated in the electrical boundary layers. Therefore, the power dissipated over the entire cross plane is given by

$$P_d = (\boldsymbol{j}\cdot\boldsymbol{j})/\Sigma + j_y uB\Delta = P - P_p \tag{20}$$

Electrical Efficiency

The electrical efficiency of an accelerator is simply the ratio of the push power to the applied power

$$\eta_a = \frac{P_p}{P} = \frac{\boldsymbol{u}\cdot(\boldsymbol{j}\times\boldsymbol{B})_x}{\boldsymbol{j}\cdot\boldsymbol{E}} = \frac{uj_yB}{IE_x/A} \tag{21}$$

It follows that the generator efficiency is defined as the reciprocal of the accelerator efficiency ($\eta_g = 1/\eta_a$).

Power Relationships

By combining the results in Table 1 with the relationships just described, it is possible to express the mean power parameters in terms of the independent variables E_x or I. These results are listed in Table 2.

Generalized Vector Diagram

It is generally instructive to examine the qualitative behavior of the internal electric fields and current densities under the assumption that MHD effects have only a slight effect on flow properties, such that the core flow region is homogeneous. In this case, the generalized Ohm's law can be used to construct representative vector diagrams for diagonalized devices, as shown in Fig. 3 for fixed values of φ.

To construct these diagrams, the generalized Ohm's law defined by Eq. (3) is put into the form

$$(\boldsymbol{j}/\Sigma) + \Omega[(\boldsymbol{j}/\Sigma)\times(\boldsymbol{B}/B)] = \boldsymbol{E}' \tag{22}$$

where we immediately recognize that the two terms on left-hand side must be orthogonal. Thus, each of these terms represents one side of a right triangle with the hypotenuse $\boldsymbol{E}'$ inclined at an angle of $\tan^{-1}\Omega$. The generalized electric field must simultaneously satisfy the vector relation defined by Eq. (2).

Figures 3a–3c show the load current dependence of a diagonalized generator ($\varphi<0$). In the open circuit case Fig. 3a, there is no current flow to the load, and the which internal current density vector must align with the diagonal link which defines planes of constant electric potential. Thus, the current is closed through the diagonal short, and $\boldsymbol{E}_y$ exactly compensates for the combined $\boldsymbol{u}\times\boldsymbol{B}$ and $\boldsymbol{E}_d$ induced potentials. Note that j_x is directed upstream under these conditions. As the load current is increased, the current density vector rotates out of the plane of the diagonal link until it aligns with the $\boldsymbol{u}\times\boldsymbol{B}$ vector. At this point, $j_x = 0$, and we arrive at the Hall current neutralized condition (Fig. 3b). If the load current is further increased, the current vector continues its rotation, and the direction of Hall current flow is reversed. Ultimately, the current density vector becomes perpendicular to the plane of the diagonal link as the electric field goes to zero at the short circuit condition (Fig. 3c).

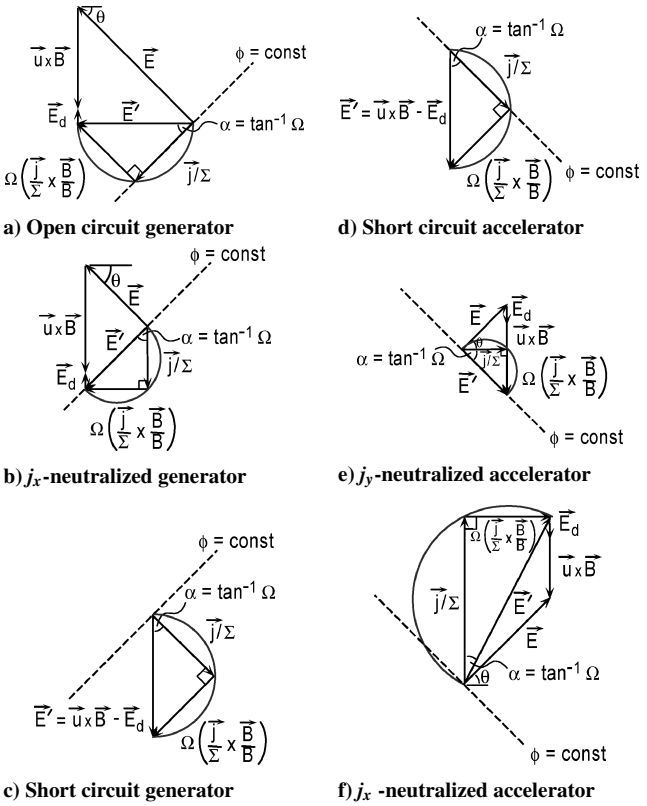

Fig. 3 Vector diagrams for crossed-field diagonal MHD devices; diagrams show relative orientation of the current density vector and electric field vectors based on the generalized Ohm's low $\boldsymbol{j}/\Sigma + \Omega(\boldsymbol{j}/\Sigma\times\boldsymbol{B}/B) = \boldsymbol{E}'$ and the generalized electric field relation $\boldsymbol{E}' = \boldsymbol{E} + \boldsymbol{u}\times\boldsymbol{B} - \boldsymbol{E}_d$.

Figures 3d–3f show the load current dependence of a diagonalized accelerator ($\phi>0$). When the applied axial electric field is zero, and there is no load current, we obtain the open circuit accelerator loading condition (Fig. 3d). The internal current density vector corresponds to the generator short circuit case under these unique circumstances. Note that $j_y<0$ (braking regime) and that the current flow is closed through the diagonal short. With increasing applied axial electric field, the current density vector rotates out of the plane of the diagonal link. The device remains in a braking regime, however, until the applied field becomes large enough to force j_y to zero, at which point we attain the zero efficiency accelerator condition (Fig. 3e). Further increases in applied current leads to continued rotation of the current density vector and increasing values of j_y. Eventually, one reaches a j_x neutralized accelerator condition (Fig. 3f). Any increase of the applied current beyond this point leads to a reversal in the direction of axial current flow, while the magnitude of the current density vector continues to grow.

Current Dependent Voltage Drop

The performance relationships previously developed hold for any fixed value of Δ. However, extensive experimental research with

Table 3 Reference conditions for variable

Mode	Δ'	Δ''	I'	I''
Generator	Δ_o	Δ_s	$I_o = 0$	I_s
Accelerator	$\Delta_z = \Delta_s$	$\Delta_n = 0$	I_z	I_n

MHD generators has clearly established that the near-electrode voltage drop is approximately linearly dependent on the transverse current density.[16–18] That is, any increase in total current leads to a proportionate increase in voltage drop. This behavior is assumed to extend to accelerator operation, as well.

The linear relationship between V_d and j_y permits the construction of a simple two-parameter model

$$V_d = [(V_d'' - V_d')/(I'' - I')](I - I') + V_d' \tag{23}$$

where the prime and double-prime superscripts indicate two distinct loading conditions. It is generally more convenient to express this relation directly in terms of Δ

$$\Delta = [(\Delta'' - \Delta')/(I'' - I')](I - I') + \Delta' \tag{24}$$

Selection of appropriate reference conditions depends on the mode of operation. For a generator, it is most natural to adopt the open circuit ($\Delta' = \Delta_o$) and short circuit ($\Delta'' = \Delta_s$) conditions on the extreme ends of the operational load line. For an accelerator, it is convenient to adopt the zero power condition, which corresponds to a short circuit generator ($\Delta' = \Delta_z = \Delta_s$), and the j_y neutralized condition ($\Delta'' = \Delta_n = 0$). The selected reference conditions are listed in Table 3. The implications of this model are now examined for both generator and accelerator modes.

Generator Mode

At the short circuit generator condition, $E_x = 0$, $I'' = I_s$, and $\Delta'' = \Delta_s$. From Table 1, we therefore deduce

$$I'' = I_s = \frac{\Sigma u B A (1 + \Delta_s)(\Omega - \varphi)}{1 + \Omega^2} \tag{25}$$

Elimination of I'' by the use of Eq. (24) immediately yields an expression for Δ in terms of I for a generator

$$\Delta = \Delta_o - \left[\frac{(1 + \Omega^2)(\Delta_o - \Delta_s)}{(\Omega - \varphi)(1 + \Delta_s)}\right]\frac{I}{\Sigma u B A} \tag{26}$$

This relationship may be used to eliminate Δ in the performance relations of Tables 1 and 2.

Accelerator Mode

The zero power open circuit accelerator condition corresponds to the short circuit generator condition with $\varphi > 0$. In this case, $E_x = 0$, $I' = I_z$, and $\Delta' = \Delta_z = \Delta_s$, and we deduce that

$$I' = I_z = \frac{\Sigma u B A (1 + \Delta_s)(\Omega - \varphi)}{1 + \Omega^2} \tag{27}$$

The point of transverse current density neutralization corresponds to a zero efficient accelerator where $j_y = 0$, $I'' = I_n$, and $\Delta'' = \Delta_n = 0$. This implies

$$I'' = I_n = \Sigma u B A/(\Omega + \varphi) \tag{28}$$

Eliminating I' and I'' in Eq. (24) gives an expression for Δ in terms of I for an accelerator

$$\Delta = \Delta_s\left[1 - \frac{(\Omega + \varphi)(1 + \Omega^2)(I/\Sigma u B A) - (\Omega^2 - \varphi^2)(1 + \Delta_s)}{(1 + \Omega^2) - (\Omega^2 - \varphi^2)(1 + \Delta_s)}\right] \tag{29}$$

This relationship may be used to eliminate Δ in the performance relations of Tables 1 and 2.

Performance Diagrams

It is possible to construct an informative performance map for DCW MHD devices following the general methodology first outlined by Powers et al., who assumed a constant voltage drop in the electrode sheath layer.[2] The significant modifications associated with a variable effective voltage drop model were later noted and described by Wu for the DCW generator case.[3] Here, Wu's analysis is explicitly extended for DCW accelerator operation as well.

Dimensionless Performance Parameters

As a first step, the governing performance relationships are simplified by definition of the following dimensionless quantities:

$$\mathcal{J} = \boldsymbol{j}/\Sigma u B, \qquad \mathcal{E} = \boldsymbol{E}/uB$$

$$\mathcal{I} = I/\Sigma u B A, \qquad \mathcal{P} = P/\Sigma u^2 B^2 \tag{30}$$

Substitution into the component form of the generalized Ohm's law then yields

$$\mathcal{J}_x = [1/(1 + \Omega^2)][\mathcal{E}_x + \Omega\mathcal{E}_y + \Omega(1 + \Delta)] \tag{31}$$

$$\mathcal{J}_y = [1/(1 + \Omega^2)][\Omega\mathcal{E}_x + \mathcal{E}_y - (1 + \Delta)] \tag{32}$$

It also follows that the electric field components can be stated explicitly in terms of current density

$$\mathcal{E}_x = \mathcal{J}_x + \Omega\mathcal{J}_y \tag{33}$$

$$\mathcal{E}_y = -\Omega\mathcal{J}_x + \mathcal{J}_y + (1 + \Delta) \tag{34}$$

An expression for the dimensionless total current is obtained from substitution of Eq. (30) into Eq. (12)

$$\mathcal{I} = \mathcal{J}_x + \varphi\mathcal{J}_y \tag{35}$$

And the dimensionless laboratory power density follows directly from substitution of Eq. (30) into Eq. (13)

$$\mathcal{P} = \mathcal{J} \cdot \mathcal{E} = \mathcal{J}_x\mathcal{E}_x + \mathcal{J}_y\mathcal{E}_y \tag{36}$$

Elimination of $\mathcal{E}_x$ and $\mathcal{E}_y$ by the use of Eqs. (33) and (34) yields the more convenient form

$$\mathcal{P} = \mathcal{J}_x^2 + \mathcal{J}_y^2 + (1 + \Delta)\,\mathcal{J}_y \tag{37}$$

Furthermore, we may define the dimensionless push power as

$$\mathcal{P}_p = P_p \big/ \Sigma u^2 B^2 = u j_y B \big/ \Sigma u^2 B^2 = j_y \big/ \Sigma u B = \mathcal{J}_y \tag{38}$$

and the electrical efficiency may be expressed in terms of dimensionless parameters by combining Eqs. (37) and (38)

$$\eta_a = \mathcal{P}_p/\mathcal{P} = \mathcal{J}_y \big/ \left[\mathcal{J}_x^2 + \mathcal{J}_y^2 + (1 + \Delta)\mathcal{J}_y\right] = 1/\eta_g \tag{39}$$

It is readily apparent that the relationships in Tables 1 and 2 can all be put in dimensionless form using Eq. (30); the results are obvious and are not tabulated. The current dependent effective voltage drop effect is accounted for with either Eq. (26) or (29) in dimensionless form.

As a prelude to the construction of the graphical performance map, it is instructive to examine performance parameter variations as a function of the dimensionless axial electric field $\mathcal{E}_x$. Figure 4, for example, summarizes calculated parameter variations under the assumption of representative values for electrical/flow conditions, material functions, and wall angle. Starting from the open circuit generator condition and gradually reducing the load impedance, we observe the sequential occurrence of all loading conditions depicted in Fig. 3.

For an open circuit generator, $I = 0$, and Eq. (35) yields the constraint $\mathcal{J}_{x,o} = -\varphi\mathcal{J}_{y,o}$. We, therefore, infer that $\mathcal{J}_{x,o} < 0$ since $\varphi < 0$ and $\mathcal{J}_{y,o} < 0$ for the assumed magnetic field direction. In this case,

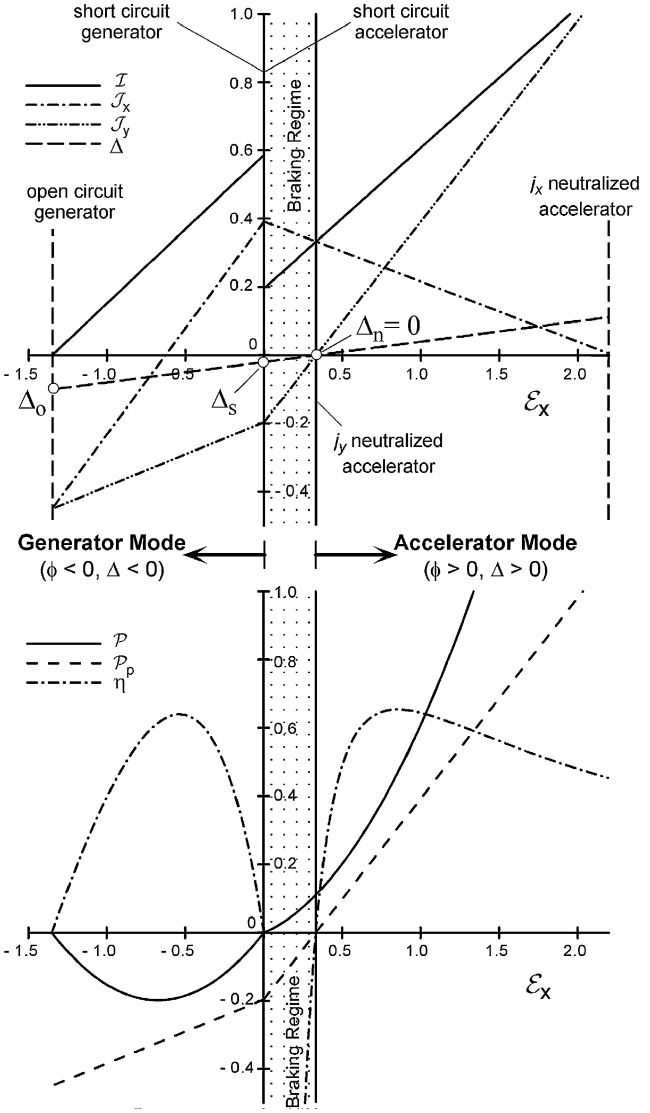

Fig. 4 Variation of performance parameters based on representative values for flow-field conditions, material functions, and wall angle: $\varphi = \pm 1$, $B = 4T$, $\Sigma = 100$, $\Omega = 2$, $u = 3$ km/s, $\Delta_o = -0.1$, and $\Delta_s = -0.02$.

the internal current is forced parallel to the wall angle and is completely shorted through the diagonal linkage. As the load impedance is decreased below a critical level, however, the total current becomes nonzero, and the negatively directed axial electric field begins to fall in magnitude.

If the load impedance is decreased all of the way to zero, we arrive at the short circuit generator condition corresponding to $\mathcal{E}_x = 0$. Here, application of Eq. (33) yields the constraint $\mathcal{J}_{x,s} = -\Omega \mathcal{J}_{y,s}$, which implies $\mathcal{J}_{x,s} > 0$ since $\Omega > 0$ and $\mathcal{J}_{y,s} < 0$. In this case, the internal current flow is forced perpendicular to the wall angle, and no current flows through the diagonal linkage.

Consideration of these open and short circuit constraints clearly implies the existence of a Hall current neutralized condition ($\mathcal{J}_x = 0$) on the generator load line. It is also clear that maximum power extraction and electrical efficiency must also occur at some point between open and short circuit conditions. This point may or may not coincide with the Hall current neutralized condition. Note that the magnitude of Δ is largest at open circuit loading where the magnitude of $\mathcal{J}_y$ is greatest.

A simple reversal of the wall angle ($\varphi > 0$) at the generator short circuit condition yields the open circuit accelerator condition. If power is then gradually applied such that a positive axial electric field is impressed on the accelerator, we enter a regime where the transverse voltage is insufficient to overcome the induced $\boldsymbol{u} \times \boldsymbol{B}$ potential, and $\mathcal{J}_y$ remains negatively directed. This is commonly referred to as the braking regime, where all applied power goes into joule heating of the working fluid. Eventually, the applied voltage becomes high enough to neutralize the transverse current, at which point $\Delta \to 0$.

An increase of the applied electric field beyond this point yields positive push work and flow acceleration. The transverse current and total current grow in magnitude, more power is delivered to the device, and Δ steadily increases. At the same time, axial current flow gradually decreases until the $\mathcal{J}_x$ neutralization condition is reached. Additional increases in applied field and power beyond this point simply reverses the direction of $\mathcal{J}_x$. Note that optimal accelerator electrical efficiency occurs at an applied electric field much less than that required to neutralize axial current flow.

Performance Map

The operational attributes of MHD devices can be exhibited in the most vivid manner on a performance map in the plane of dimensionless current density and electric field. Following the methodology of Powers et al.,[2] as modified by Wu for current dependent voltage drop,[3] we complete the square in Eq. (37) to obtain the family of circles defined by

$$\mathcal{J}_x^2 + \{\mathcal{J}_y + [(1+\Delta)/2]\}^2 = \mathcal{P} + [(1+\Delta)/2]^2 \tag{40}$$

These circles are centered at $\mathcal{J}_x = 0$, $\mathcal{J}_y = (1+\Delta)/2$, with a radius of $\{\mathcal{P} + [(1+\Delta)/2]^2\}^{1/2}$.

Transformation to the $\mathcal{E}_x, \mathcal{E}_y$ axes is defined by Eqs. (33) and (34), and the origin of the $\mathcal{E}_x, \mathcal{E}_y$ axes in the $\mathcal{J}_x, \mathcal{J}_y$ plane follows directly from Eqs. (31) and (32)

$$\mathcal{J}_{x,\varepsilon=0} = \Omega(1+\Delta)/(1+\Omega^2), \qquad \mathcal{J}_{y,\varepsilon=0} = -(1+\Delta)/(1+\Omega^2) \tag{41}$$

The locus of points defining this origin can be expressed independent of Ω by combination of Eqs. (33) and (34) under the condition $\mathcal{E}_x = \mathcal{E}_y = 0$

$$\mathcal{J}_{x,\varepsilon=0}^2 + \{\mathcal{J}_{y,\varepsilon=0} + [(1+\Delta)/2]\}^2 = [(1+\Delta)/2]^2 \tag{42}$$

Note that the circles defined by Eq. (40) reduce to the loci defined by Eq. (42) at zero power density. Thus, the generator boundary coincides with the locus of the origin of the $\mathcal{E}_x, \mathcal{E}_y$ axes, and all power generating circles lie inside this boundary because $\mathcal{P} < 0$ for a generator. Further insight may be gained through examination of extreme generator loading conditions.

At generator short circuit, the Hall field goes to zero and Eq. (33) gives the constraint

$$\mathcal{J}_{x,s} = -\Omega \mathcal{J}_{y,s} \Rightarrow \tan^{-1}(-1/\Omega) = \mathcal{J}_{y,s}/\mathcal{J}_{x,s} \tag{43}$$

Because $\Omega > 0$ and $\mathcal{J}_y < 0$, given the assumed magnetic field orientation, the short circuit operating domain resides in the fourth quadrant of the current density plane.

At generator open circuit conditions, the total current falls to zero, and Eq. (35) gives the constraint

$$\mathcal{J}_{x,o} = -\varphi \mathcal{J}_{y,o} \Rightarrow \tan^{-1}(-1/\varphi) = \mathcal{J}_{y,o}/\mathcal{J}_{x,o} \tag{44}$$

Because $\varphi < 0$ and $\mathcal{J}_y < 0$ for the generator mode, the open circuit operating domain resides in the third quadrant of the current density plane.

Clearly, the power density vanishes at both open and short circuit conditions, but the critical discriminating factor to note is that Δ varies with current over the entire load range ($-1 < \Delta_o < \Delta_s < 0$). Therefore, the radius of the zero power circle depends on the load. The zero power loci for short and open circuit loading follows from Eq. (40) with $\mathcal{P} = 0$

$$\mathcal{J}_{x,s}^2 + \{\mathcal{J}_{y,s} + [(1+\Delta_s)/2]\}^2 = [(1+\Delta_s)/2]^2 \tag{45}$$

$$\mathcal{J}_{x,o}^2 + \{\mathcal{J}_{y,o} + [(1+\Delta_o)/2]\}^2 = [(1+\Delta_o)/2]^2 \tag{46}$$

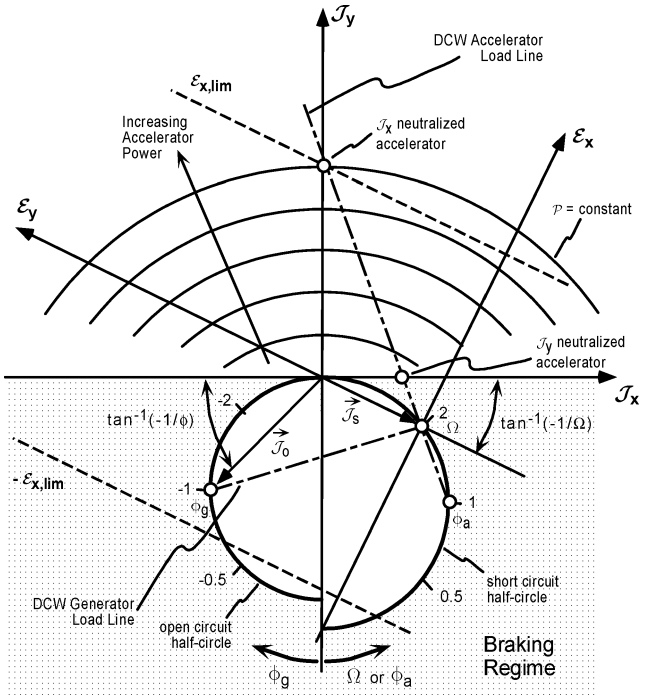

Fig. 5 Performance map for diagonal conducting wall MHD devices with current-dependent voltage drop effect.

With these expressions, it is possible to construct the short and open circuit half-circles. The short circuit half-circle is centered at $\mathcal{J}_x = 0$, $\mathcal{J}_y = (1 + \Delta_s)/2$ with radius $(1 + \Delta_s)/2$, and the open circuit half-circle is centered at $\mathcal{J}_x = 0$, $\mathcal{J}_y = (1 + \Delta_o)/2$ with radius $(1 + \Delta_o)/2$. These loci are illustrated in Fig. 5 where the load line connects in accordance with the constraints defined by Eqs. (43) and (44). Because $\Delta_o < \Delta_s$, the radius of the open circuit half-circle is smaller than the radius of the short circuit half-circle and the center points are shifted.

The origin of the $\mathcal{E}_x$, $\mathcal{E}_y$ axes falls on the short circuit half-circle at the points defined by Eq. (41). Inspection of Eq. (34) indicates that the $\mathcal{E}_y$ axes passes through the origin of the $\mathcal{J}_x$, $\mathcal{J}_y$ axes because $\Delta = 0$ at this condition. The various points of interest are indicated on the diagram.

Combination of the DCW electric field constraint defined by Eq. (10) with Eqs. (30), (33), and (34) yields an expression for the operating load line in the form

$$(\Omega + \varphi)\mathcal{J}_x + (\Omega\varphi - 1)\mathcal{J}_y = 1 + \Delta \tag{47}$$

It is now possible to eliminate Δ by the use of either Eq. (26) for a generator or Eq. (29) for an accelerator. In both case, one ends up with an equation for a line in the $\mathcal{J}_x$, $\mathcal{J}_y$ plane because Δ is linearly related to $\mathcal{J}_x$ and $\mathcal{J}_y$. The resulting operating lines are illustrated in Fig. 5.

In the generator case, the operating line passes through the short and open circuit load conditions, as determined by Eqs. (43) and (44), respectively. In the accelerator case, the operating line originates from the generator short circuit loading point on the zero power half-circle. This line also projects through a point on the half-circle defined by the value of φ.

The $\mathcal{P}$ circles for accelerator operation are obtained from Eq. (40) when Eq. (29) is used to eliminate Δ. Note that the accelerator operates in the dissipative braking regime between open circuit and zero efficiency conditions. Thus, positive push work is obtained only when the power density exceeds that associated with the zero efficiency condition where $\mathcal{J}_y = \eta_a = \Delta_n = 0$

$$\mathcal{P}_{\eta_a = 0} = \mathcal{J}_x\mathcal{E}_x = [(1 + \Delta_n)/(\Omega + \varphi)]^2 = 1/(\Omega + \varphi)^2 \tag{48}$$

Portions of the constant-$\mathcal{P}$ circles lying within the positive push work regime are illustrated in Fig. 5. Inspection of Eq. (40) reveals that the radii of these circles are larger than would occur for an ideal device in which there is no parasitic voltage drop ($\Delta = 0$). Thus, additional power must be applied in a real device to achieve a desired intensity of acceleration.

Note that the optimum accelerator efficiency occurs with a finite axial current. Increasing the accelerator power density until $\mathcal{J}_x$ vanishes will inevitably reduce the electrical efficiency below the optimal value. In fact, to accelerate plasma efficiently (with little heat production), it is desirable to maintain gentle acceleration levels by keeping the back emf only slightly less than the applied electric field. In practice, the added length and weight associated with gentle acceleration must be traded against the electrical inefficiencies encountered with high push power.

For a generator, the maximum power condition can differ considerably from the maximum efficiency condition. Furthermore, maximum generator efficiency operation also occurs with a finite axial current (Fig. 4). It should be pointed out that achieving optimal power generation for a given value of Hall parameter depends on careful selection of the wall angle. This is examined for the sake of completeness.

By definition, the dimensionless power density may be expressed in the form

$$\mathcal{P} = P/\Sigma u^2 B^2 = (I E_x/A)/\Sigma u^2 B^2 = \mathcal{I}\mathcal{E}_x = (\mathcal{J}_x + \varphi\mathcal{J}_y)\mathcal{E}_x \tag{49}$$

If we now use Eq. (26) to eliminate $\mathcal{I}$ in the appropriate expressions for $\mathcal{J}_x$, $\mathcal{J}_y$, and $\mathcal{E}_x$, we obtain the dimensionless generator power density in terms of Δ

$$\mathcal{P} = \frac{(\Omega - \varphi^2)(1 + \Delta_s)^2}{(1 + \varphi^2)(1 + \Omega^2)}\left(\frac{\Delta - \Delta_o}{\Delta_s - \Delta_o}\right)\left[\frac{\Delta - \Delta_o}{\Delta_s - \Delta_o} - \frac{1 + \Delta}{1 + \Delta_s}\right] \tag{50}$$

The maximum power density is defined by the constraint $\partial\mathcal{P}/\partial\Delta = 0$, which yields the relation

$$\Delta_{\max} = (\Delta_o + \Delta_s)/2 \tag{51}$$

Substitution of this result into Eq. (50) then yields

$$\mathcal{P}_{\max} = \frac{-(\Omega - \varphi^2)}{(1 + \varphi^2)(1 + \Omega^2)}\frac{(1 + \Delta_s)(1 + \Delta_o)}{4} \tag{52}$$

Thus, $\mathcal{P}_{\max}$ depends on φ, and the optimal wall angle for a given Hall parameter is determined by the constraint $\partial\mathcal{P}_{\max}/\partial\varphi = 0$ which leads to the design criterion

$$\Omega\varphi = -1 \tag{53}$$

If this criterion is enforced, we find the maximum possible generator power density to be

$$\mathcal{P}_{\max(\Omega\varphi = -1)} = -[(1 + \Delta_s)(1 + \Delta_o)]/4 \tag{54}$$

Electrode Boundary-Layer Effects

The effective voltage drop arises from cold wall boundary-layer effects, including gasdynamic variations, finite segmentation, discharge constriction, and electrode falls. Because fluid temperature and velocity vary rapidly as they approach the wall, the conductivity and induced voltage also exhibit strong variations in the thermal and momentum boundary layers, respectively. Furthermore, the rapid decrease in temperature near the electrode surface leads to breakdown and a sudden switch from diffuse current transport to constricted arcs. Current attachment to cold electrodes almost always occurs through a thin layer of short arcs.

The basic boundary-layer features are shown in Fig. 6 for an accelerator configuration. For simplicity, the thermal and momentum boundary layers are both assumed to have a thickness δ. In addition, current constriction is indicated at the electrode surface where attachment occurs through short arcs spanning the anode thickness δ_a and the cathode thickness δ_c. Note that Fig. 6 shows a concentration of current due to the Hall effect at the upstream end of the cathode and the downstream end of the anode in accordance with experimental observations for accelerators.[19,20]

The effective electrode voltage drop V_d is defined as the potential difference by which the voltage between opposite electrodes is

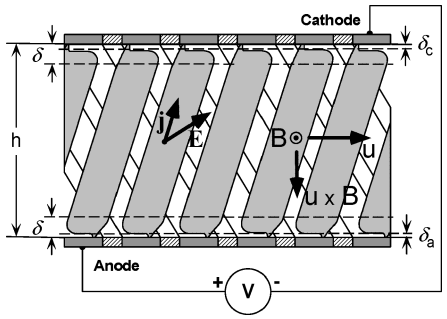

Fig. 6 Current transport and boundary-layer dimensions for a diagonal conducting wall cross-field accelerator.

increased (due to boundary-layer effects) with respect to the fully homogeneous case. The increase in V_d is quantified through an integration of the transverse electric field defect across the electrode boundary layers. For convenience, V_d is split into the following separate components:

$$V_d = V_a + V_c + V_g \tag{55}$$

where the anode voltage fall V_a, the cathode voltage fall V_c, and the gasdynamic voltage drop V_g are defined by

$$V_a = \int_0^{\delta_a} (E_y - E_{y0})\,\mathrm{d}y$$

$$V_c = \int_{h-\delta_c}^{h} (E_y - E_{y0})\,\mathrm{d}y$$

$$V_g = \int_{\delta_a}^{\delta} (E_y - E_{y0})\,\mathrm{d}y + \int_{h-\delta}^{h-\delta_c} (E_y - E_{y0})\,\mathrm{d}y \tag{56}$$

Note that the zero subscript refers to the homogeneous core flow conditions.

Factors contributing to the anode and cathode voltage falls include the arc attachment region and the potential associated with electron emission from cold electrode material. In general, the voltage drop in the arc columns is negligible because the arc length is small compared to the boundary-layer thickness, and the anode electrode fall is negligible because it does not have to emit electrons. Thus, $V_a \approx 0$. The cathode does emit electrons, however, and the voltage drop associated with this process can only be approximated in an empirical fashion. For most materials, $V_c \approx 10$–20 V.

The gasdynamic voltage drop may be evaluated by application of the generalized Ohm's law in the boundary layer to eliminate E_y. In this particular case, the appropriate form for E_y may be obtained from Eq. (9) by neglecting Δ

$$E_y = [(1+\Omega^2)/\Sigma]j_y - \Omega E_x + uB \tag{57}$$

If Ω is invariant, V_g takes the form

$$V_g = \int_{\delta_a}^{\delta} \left\{ \left[\frac{j_y}{\Sigma/1+\Omega_0^2} + uB \right] - \left[\frac{j_y}{\Sigma_0/1+\Omega_0^2} + u_0 B \right] \right\} \mathrm{d}y + \int_{h-\delta}^{h-\delta_c} \left\{ \left[\frac{j_y}{\Sigma/1+\Omega_0^2} + uB \right] - \left[\frac{j_y}{\Sigma_0/1+\Omega_0^2} + u_0 B \right] \right\} \mathrm{d}y \tag{58}$$

and it is convenient to split V_g into two parts

$$V_\Sigma = \frac{2j_y}{\Sigma_0'} \int_{\delta_a}^{\delta} \left[\frac{\Sigma_0'}{\Sigma'} - 1 \right] \mathrm{d}y \tag{59}$$

$$V_u = 2u_0 B \int_{\delta_c}^{\delta} \left[\frac{u}{u_0} - 1 \right] \mathrm{d}y \tag{60}$$

where V_Σ and V_u account separately for the decrease of Σ and induced voltage in the boundary layer and $\Sigma' = \Sigma/(1+\Omega_0^2)$. These integrals may be further simplified by defining $\xi = y/\delta$ and assuming that $\delta_a = \delta_c$

$$V_\Sigma = \frac{2\delta j_y}{\Sigma_0'} \int_{\xi_c}^{1} \left[\frac{\Sigma_0'}{\Sigma'} - 1 \right] \mathrm{d}\xi \tag{61}$$

$$V_u = 2\delta u_0 B \int_{\xi_c}^{1} \left[\frac{u}{u_0} - 1 \right] \mathrm{d}\xi \tag{62}$$

The lower limit of integration $\xi_c = \delta_c/\delta$ is the distance from the electrode surface where the current becomes constricted.

Evaluation of these integrals is facilitated by the introduction of model boundary-layer profiles for velocity and temperature.[21] For example, the velocity profile in a turbulent boundary layer is well approximated by the power law $u/u_0 = (y/\delta)^{1/n}$ where $n \approx 7$. If this relation is substituted into the integral for V_u, and $\xi_c = 0$ is used as the lower limit of integration (because u goes to zero at the wall), we obtain

$$V_u \approx 2u_0 B\delta/(1+n) \tag{63}$$

Evaluation of the integral for V_Σ is complicated by the fact that Σ_0'/Σ' increases steeply near the cold electrode surface, which makes the integral extremely sensitive to the lower limit of integration. It is assumed that electrical breakdown leading to arc attachment occurs when j_y/Σ' exceeds the critical electric field strength E_c. In this case, the limit ξ_c corresponds to a critical conductivity ratio ω_c

$$\omega_c = \Sigma_c'/\Sigma_0' = (j_y/E_c)/\Sigma_0' \tag{64}$$

Experience shows that, very near the wall the thermal boundary layer may be approximated by the power law $T/T_0 = (y/\delta)^{1/m}$, where $m = 18$–25. Furthermore, it has also been established that the electrical conductivity can be approximated by the simple power law $\Sigma'/\Sigma_0' = (T/T_0)^a (p/p_0)^b$ where $a \approx 10$–20 and $b = -\frac{1}{2}$. Thus, for negligible pressure variations, the integral for V_Σ can be expressed in the simplified form

$$V_\Sigma = \frac{2\delta j_y}{\Sigma_0'} \int_{\xi_c}^{1} [\xi^{-a/m} - 1]\,\mathrm{d}\xi \tag{65}$$

The calculation procedure is as follows. For a given value of j_y/Σ_0' and a specified E_c, it is possible to compute ω_c, which may be used in turn to compute $T_c/T_0 = \omega_c^{1/a}$. Then, the lower limit of integration may be determined from the relation $\xi_c = (T_c/T_0)^m$, and the integral of Eq. (65) may be evaluated. For illustrative purposes, calculated values for ξ_c and $V_\Sigma/2\delta$ are shown in Fig. 7 as a function

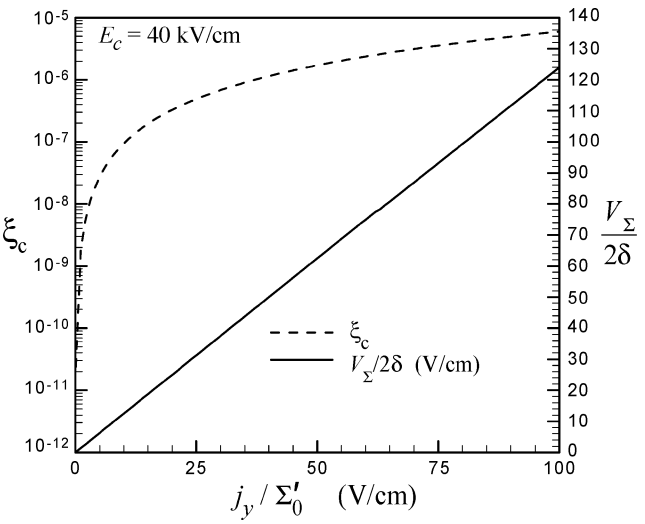

Fig. 7 Variation of ξ_c and $V_\Sigma/2\delta$ as a function of j_y/Σ_0': $E_c = 40$ kV/cm, $n = 7$, $m = 18$, and $a = 10$.

of j_y/Σ_0', given $E_c = 40$ kV/cm, $n = 7$, $m = 18$, and $a = 10$. Note that $V_\Sigma \propto j_y$, in accordance with empirical observations.

Practical Design Constraints

In a real device, practical design constraints limit the available operating range. The axial electric field, for instance, must be limited due to breakdown considerations. If the axial electric field becomes too large, interelectrode arcing can occur, and the resulting shorts can degrade device performance. Furthermore, high heat dissipation in these concentrated arc discharges can cause severe erosion of wall material and dramatic reduction in channel operating life.

Experience has shown that a realistic upper limit for the axial electric field is no more than 100 V/cm. The existence of such a design constraint is shown by the dashed lines marked $\pm\mathcal{E}_{x,\mathrm{lim}}$ on the performance map of Fig. 5. This implies that DCW accelerators operating with large Ω are confined to low power density operation. High power densities are attainable with low Ω at the expense of decreased efficiency.

An additional design constraint arises from the observation that excessive heat generation and material erosion will occur if the current density entering the electrode surface becomes too large. The actual limiting value depends on electrode material and geometry, but experience indicates good channel durability for values up to about 10 A/cm^2. For high power density applications having short lifetime requirements, this value can be exceeded considerably.

Conclusions

The classical cross-plane-averaged performance theory for diagonal conducting wall MHD accelerators has been extended to include a current dependent sheath layer voltage drop. This approach yields analytical performance relationships and diagrams that can be used to illuminate the rudimentary behavior of these devices and underscore the fundamental interplay of basic parameters. This simplified theoretical treatment is not intended for detailed performance prediction of practical devices, but rather to aid in the development of an intuitive understanding of device operation of general value to analysts, designers, and experimentalists alike. Despite its limitations, the theory can be extremely useful in defining anticipated performance ranges while it accounts for critical nonideal effects.

Acknowledgments

The author expresses his thanks to John T. Lineberry, President, LyTec, LLC; Y. C. L. Susan Wu, Professor (retired), University of Tennessee; and Valentin A. Bityurin, Head of Magnetohydrodynamic (MHD) Programs, Institute of High Temperatures of the Russian Academy of Sciences, for valuable discussions and for clarifying basic conceptual ideas underlying MHD performance theory.

References

[1]Litchford, R. J., Cole, J. W., Lineberry, J. T., Chapman, J. N., Schmidt, H. J., and Lineberry, C. W., "Magnetohydrodynamic Augmented Propulsion Experiment: I. Performance Analysis and Design," AIAA Paper 2002-2184, 2002.

[2]Powers, W. L., Dicks, J. B., and Snyder, W. T., "Graphical Presentation of MHD Accelerator and Generator Performance Characteristics," *AIAA Journal*, Vol. 5, No. 12, 1967, pp. 2232–2236.

[3]Wu, Y. C. L., "Performance Theory of Diagonal Conducting Wall MHD Generators," *AIAA Journal*, Vol. 14, No. 10, 1976, pp. 1362–1368.

[4]Buende, R., Muntenbruch, H., Raeder, J., Volk, R., and Zankl, G., *MHD Power Generation: Selected Problems of Combustion MHD Generators*, edited by J. Raeder, Springer-Verlag, Berlin, 1975.

[5]Bityurin, V. A., Zatelepin, V. N., and Lyubimov, G. A., "A Consideration of Some Three-Dimensional Effects in MHD Channels," *Proceedings of 16th Symposium on Engineering Aspects of Magnetohydrodynamics (SEAM)*, May 1977.

[6]Ahluwalia, R. K., Vanka, S. P., Im, K. H., and Zwick, S. A., "Formulation and Assessment of a Cross-Plane Electrical Model for Magnetohydrodynamic Channels," *Journal of Energy*, Vol. 6, No. 5, 1982, pp. 314–322.

[7]de Montardy, A., "MHD Generator with Series-Connected Electrodes," *Proceedings of the International Symposium on MHD Electrical Power Generation*, Newcastle upon Tyne, England, Paper 19, Sept. 1962.

[8]Dicks, J. B., "Design and Operation of Open Cycle Hall Current Neutralized MHD Accelerators and Generators with Diagonal Conducting Strip Walls," *Proceedings of 5th Symposium on Engineering Aspects of Magnetohydrodynamics (SEAM)*, April 1964.

[9]Dicks, J. B., "Improvements in Design of MHD Accelerator Channels for Aerodynamic Purposes," in *Arc Heaters and MHD Accelerators for Aerodynamic Purposes*, AGARDograph 84: Supplemental Volume, *Proceedings of AGARD Specialists Meeting*, AGARD, 1964, pp. 127–174.

[10]Schlueter, A., "Dynamik des Plasmas I," *Zeitschrift für Naturforschung*, Vol. 5a, 1950, p. 72; also Vol. 6a, 1951, pp. 73–78.

[11]Cowling, T. G., *Magnetohydrodynamics*, Interscience, New York, 1957, Chap. 6, p. 107.

[12]Sherman, A., "The Generalized Ohm's Law for a Partially Ionized Gas," Internal Report DF59FPD-807, General Electric Company, Oct. 1959.

[13]Polovin, R. V., and Cherkasova, K. P., "Magnetohydrodynamic Description of a Plasma," *Soviet Physics—Technical Physics*, Vol. 7, No. 6, 1962, pp. 475–479.

[14]Liubimov, G. A., "On the Form of Ohm's Law in Magnetohydrodynamics," *Soviet Mathematics: Applied Mathematics and Mechanics*, Vol. 25, No. 4, 1962, pp. 913–929.

[15]Rosa, R. J., "Hall and Ion Slip Effects in a Nonuniform Gas," *Physics of Fluids*, Vol. 5, No. 9, 1962, pp. 1081–1090.

[16]Wu, Y. C. L., Dicks, J. B., Crawford, L. W., Muehlhauser, J. W., Scott, M. A., and Sood, N., "Theoretical and Experimental Studies of MHD Power Generation with Char," *Proceedings of 12th Symposium on Engineering Aspects of Magnetohydrodynamics (SEAM)*, 1972, pp. II.1.1–II.1.14.

[17]Wu, Y. C. L., Rajogopal, G., and Dicks, J. B., "Investigation of Open-Cycle MHD Power Generation," AIAA Paper 74-175, Jan. 1974.

[18]Shanklin, R. V., III, and Nimmo, R. A., "Report on the Status and Results of the KIVA-I Open Cycle MHD Generator System," *Proceedings of 14th Symposium on Engineering Aspects of Magnetohydrodynamics (SEAM)*, 1974, pp. I.8.1–I.8.5.

[19]Demetriades, S. T., and Lenn, P. D., "Electrical Discharge Across a Supersonic Jet of Plasma in Transverse Magnetic Field," *AIAA Journal*, Vol. 1, No. 1, 1963, pp. 234–236.

[20]Denison, M. R., and Zeimer, R. W., "Investigation of the Phenomena in Cross-Field Plasma Accelerators," in *Physico-Chemical Diagnostics of Plasmas*, edited by T. P. Anderson, R. W. Springer, and R. C. Warder, Northwestern Univ. Press, Evanston, IL, 1964, pp. 201–232.

[21]Schlichting, H., *Boundary Layer Theory*, 6th ed., McGraw–Hill, New York, 1968.